TÜBİTAK

Turkish Journal of Chemistry

http://journals.tubitak.gov.tr/chem/

Research Article

Turk J Chem
(2017) 41: 426 – 439

doi:10.3906/kim-1607-5

Microwave-enhanced Fenton-like degradation by surface-modified metal–organic frameworks as a promising method for removal of dye from aqueous samples

Seyed Ershad MORADI[1], **Shayessteh DADFARNIA**[1,*], **Ali Mohammad HAJI SHABANI**[1], **Saeed EMAMI**[2]

[1]Department of Chemistry, Faculty of Science, Yazd University, Yazd, Iran

[2]Department of Medicinal Chemistry and Pharmaceutical Sciences Research Center, Faculty of Pharmacy, Mazandaran University of Medical Sciences, Sari, Iran

Received: 03.07.2016 • **Accepted/Published Online:** 01.07.2017 • **Final Version:** 16.06.2017

Abstract: In the current research, the sulfonated metal–organic framework loaded on iron oxide nanoparticles, Fe_3O_4@MIL-100(Fe)-OSO_3H, has been synthesized and utilized as a Fenton-like catalyst for the decolorization of aqueous solutions containing methyl orange (MO) dye as a model organic pollutant. The morphology and structure of the catalyst were characterized by X-ray powder diffraction, transmission electron microscopy, Brunauer–Emmett–Teller analysis, thermogravimetric analysis, Fourier transform infrared spectroscopy, and UV-Vis diffuse reflectance spectroscopy. The effects of various parameters on MO degradation were investigated and the optimum conditions for MO degradation were found to be an initial concentration of MO of 100 mg/L, initial concentration of H_2O_2 of 40 mg/L, pH 3.0, and microwave power of 500 W. The results indicated that the removal of the MO was fast; the kinetic data followed a pseudo first-order model and under microwave irradiation time of 6 min it degraded up to 99.9%. Thus, microwave-induced Fenton-like degradation using Fe_3O_4@MIL-100(Fe)-OSO_3H is a promising technology for the removal of dye from wastewater.

Key words: Microwave-induced Fenton-like degradation, methyl orange; metal–organic frameworks, iron oxide nanoparticles, sulfonation

1. Introduction

Dyes are synthetic aromatic organic compounds that are widely used in the textile industry.[1] They are mostly nonbiodegradable,[2] they pose a serious threat to aquatic life, and some of them are known to have serious genotoxic effects on humans.[2] Methyl orange (MO) ($C_{14}H_{14}N_3NaO_3S$) is extensively used as an indicator in laboratories. It is also used in paper manufacturing, textile, printing, pharmaceutical, and food industries.[3] The effluents of industries containing MO dyes are discharged into water bodies, causing many health hazards.[2]

Various physical, chemical, and biological methods such as adsorption.[4] coagulation,.[5] reverse osmosis,[6] sonochemical degradation,[7] photocatalytic degradation,[8] advanced oxidation processes (AOPs) with UV/H_2O_2,[9] electrochemical oxidation,[10] catalytic oxidation,[11] and wet air oxidation[12] have been used for the decolorization of dye from wastewater. In recent years, AOPs[13] have drawn significant attention to the mineralization of dyes. The Fenton-like reaction is a well-studied AOP that uses hydrogen peroxide or persulfate in the presence of transition metal ions (Co, Cu, and Mn ions and Fe^{3+}).[14] The key step in the Fenton-like reaction is the formation of hydroxyl radicals ($HO^{\cdot}$) from H_2O_2 and Fe(II).[9] This technique has been used for the oxidation

*Correspondence: sdadfarnia@yazd.ac.ir

of different organic materials. The Fenton-like reaction is a developing advanced oxidation technology for the treatment of industrial wastewater containing nonbiodegradable organic pollutants.[9] Fenton-like processes can be performed in homogeneous or heterogeneous mode; the heterogeneous mode has the advantage of ease of catalyst separation from the treated sample without production of iron sludge. However, the efficiency of treatment with heterogeneous Fenton-like catalysts alone is not very good and it requires external energy.[15] In this regard, irradiation with various sources including ultraviolet light,[16] ultrasound,[17] and microwave[15] energy has been used for increasing the efficiency and speed of the heterogeneous catalyst Fenton-like reaction.[18,19] Among these sources of energy, irradiation of the Fenton-like reaction with microwave (MW) energy is one of the most promising technologies used for the degradation of organic pollutants.[15] Microwaves with wavelength between 1.0 mm and 1.0 m provide rapid heating of materials and may offer a potential solution to the kinetic problems of photodegradation technology. Microwave irradiation causes rapid rotation of the polar molecule in the solution, brings about a thermal effect, and consequently heats the solution. Microwave irradiation can also change the thermodynamic behavior of the system by weakening the chemical bond intensities of molecules and reducing the activation energy of reaction.[20] Recently, it was demonstrated that microwaves as the source of energy provide better degradation efficiency than traditional treatment methods.[21]

The application of nanomaterials as heterogeneous catalysts in water purification has attracted considerable attention.[22,23] However, due to some problems such as limited specific surface area and poor quantum efficiency, nanomaterials have low adsorption as well as degradation capacity, which must be solved for extending their application.[24] These deficiencies have been overcome through the use of nanoporous materials with high surface area or nanosized catalysts fixed on porous materials such as SiO_2,[25] ZrO_2,[26] and zeolites.[27,28] However, the introduction of new nanoporous photocatalyst systems with improved activities is still a challenging issue.

Metal–organic frameworks (MOFs) are an interesting class of porous crystalline materials that are constructed from metal ions and polyfunctional organic ligands.[29] They have attracted significant research interest in catalysis,[30] adsorption and separation,[31] gas storage,[32] and drug delivery.[33] Compared with the traditional porous materials, MOFs are synthesized under relatively milder conditions and can allow systematic engineering of the chemical and physical properties through the modification of their components. Moreover, when exposed to light, MOFs can behave as photocatalysts.[34] Garcia et al. demonstrated for the first time that MOF-5 can act as an active photocatalyst for the photodegradation of phenol.[35] Later it was also shown that MOFs can also act as photocatalysts for the decolorization of organic contaminates.[36–38] Among various MOFs, iron-based materials of Institut Lavoisier (MILs) are of special interest as they are nontoxic and stable in water. Recently, the photocatalytic performances of MOFs have been improved through their modification with functional groups like amino[39] and metal nanoparticles.[40] Iron oxide nanoparticle-loaded metal organic frameworks, Fe_3O_4@MIL100(Fe), have been synthesized and used as the photocatalysts for methylene blue and rhodamine B degradation.[41]

According to our literature survey, a few studies have been carried out on the degradation of organic compounds using microwave irradiation,[15,42] while there are no reports on the combination of microwave irradiation and surface-modified MOFs for the catalytic degradation of organic pollutants. Furthermore, it has been proven that surface modification of catalysts with different sulfur-based anions enhances the acidity, thermal stability, and mesoporosity of the catalysts.[43] Thus, it is expected that surface modification of MOF photocatalysts by sulfonated groups may enhance environmental pollutant remediation. The purpose of this

study was to employ the combination of microwave and modified MOFs with a sulfonate group and Fe_3O_4 nanoparticles as a Fenton-like catalyst for the decolorization of aqueous solutions containing MO dye as the target organic pollutant. For this purpose, the Fe_3O_4@MIL-100(Fe)-OSO_3H composite, as a model MOF, was prepared and characterized by X-ray diffraction (XRD), transmission electron microscopy (TEM), Brunauer–Emmett–Teller (BET) analysis, Fourier transform infrared (FT-IR) spectroscopy, and UV-Vis diffuse reflectance spectroscopy (DRS). The variables affecting the microwave-enhanced degradation process such as catalyst concentration, microwave power, initial concentrations of MO, initial H_2O_2 concentration, and solution pH were optimized. Finally, the kinetics and mechanism of MO degradation by Fe_3O_4@MIL-100(Fe)-OSO_3H under microwave irradiation were investigated and discussed.

2. Results and discussion

2.1. Textural characterization

The XRD pattern and FT-IR spectrum of Fe_3O_4@MIL-100(Fe)-OSO_3H were compared to those of the Fe_3O_4 NPs, MIL-100(Fe) and Fe_3O_4@MIL-100(Fe), of our previous study.[44] As demonstrated, the XRD pattern of Fe_3O_4@MIL-100(Fe) (Figure 1a) has the characteristic peaks of both Fe_3O_4 and MIL-100(Fe) indicating the right synthesis of Fe_3O_4@MIL-100(Fe).[44] Moreover, Fe_3O_4@MIL-100(Fe)-OSO_3H (Figure 1a) has almost similar 2Θ values as Fe_3O_4@MIL-100(Fe) but the intensities of peaks are decreased and the peaks are broadened. This observation indicates the right modification of the sorbent as well as a decrease in the size of the particle.

The FT-IR spectrum of the Fe_3O_4@MIL-100(Fe)-OSO_3H catalyst is presented in Figure 1b. In this spectrum, the absorption band at 1685 cm^{-1} (C=O stretching band), the band at 1284 cm^{-1} (O–C–O stretching band), and the band at 732 cm^{-1} (out-of-plane bending vibrations of benzene rings) are associated with the presence of organic parts of MOFs. The two bands at 1088 and 1125 cm^{-1} are the characteristic frequencies of O=S=O stretching in SO_3H and SO_3^- stretching, respectively. The broad band at 3539 cm^{-1} is due to the contribution of the OH groups of sulfonic acid. Furthermore, comparison of FT-IR spectrum of Fe_3O_4@MIL-100(Fe)-OSO_3H (Figure 1b) with our previously reported spectra of Fe_3O_4 NPs MIL-100(Fe) and Fe_3O_4@MIL-100(Fe) [44] revealed the presence of the Fe_3O_4 NP band (578 cm^{-1} Fe-O band) in Fe_3O_4@MIL-100(Fe)-OSO_3H. Thus, the FT-IR spectra confirms the right synthesis of Fe_3O_4@MIL-100(Fe)-OSO_3H.

Furthermore, the TEM images of the Fe_3O_4@MIL-100(Fe)-OSO_3H catalyst (Figure 1c) clearly show that the catalyst particles are spherical and have a core–shell structure.

The porosity and specific surface area of MOFs have been investigated. The nitrogen adsorption–desorption isotherms of the MIL-100(Fe) and Fe_3O_4@MIL-100(Fe)-OSO_3H (Figure 2a) exhibit a type I isotherm according to IUPAC classification, representative of microporous solids. The BET surface areas and pore volumes of MIL-100(Fe) before and after modification with iron oxide nanoparticles and sulfonate group were measured. The specific surface area (S_{BET}) and micropore volume of the MIL-100(Fe) are 2352 m^2/g and 0.90 cm^3/g, respectively. The specific surface area and micropore volume of Fe_3O_4@MIL-100(Fe)-OSO_3H are reduced to 1124 m^2/g and 0.52 cm^3/g. This could be due to the incorporation of Fe_3O_4 nanospheres and surface modification of MOFs by the sulfonate group resulting in blockage of some MOF pores.

To estimate the amount of iron oxide in the structure of Fe_3O_4@MIL-100(Fe)-OSO_3H, TGA of Fe_3O_4, Fe_3O_4@MIL-100(Fe)-OSO_3H, and MIL-100(Fe) was conducted. Figure 2b shows the TGA curves of Fe_3O_4, Fe_3O_4@MIL-100(Fe)-OSO_3H, and MIL-100(Fe). The TGA curve of Fe_3O_4 clearly indicated that about 97.0

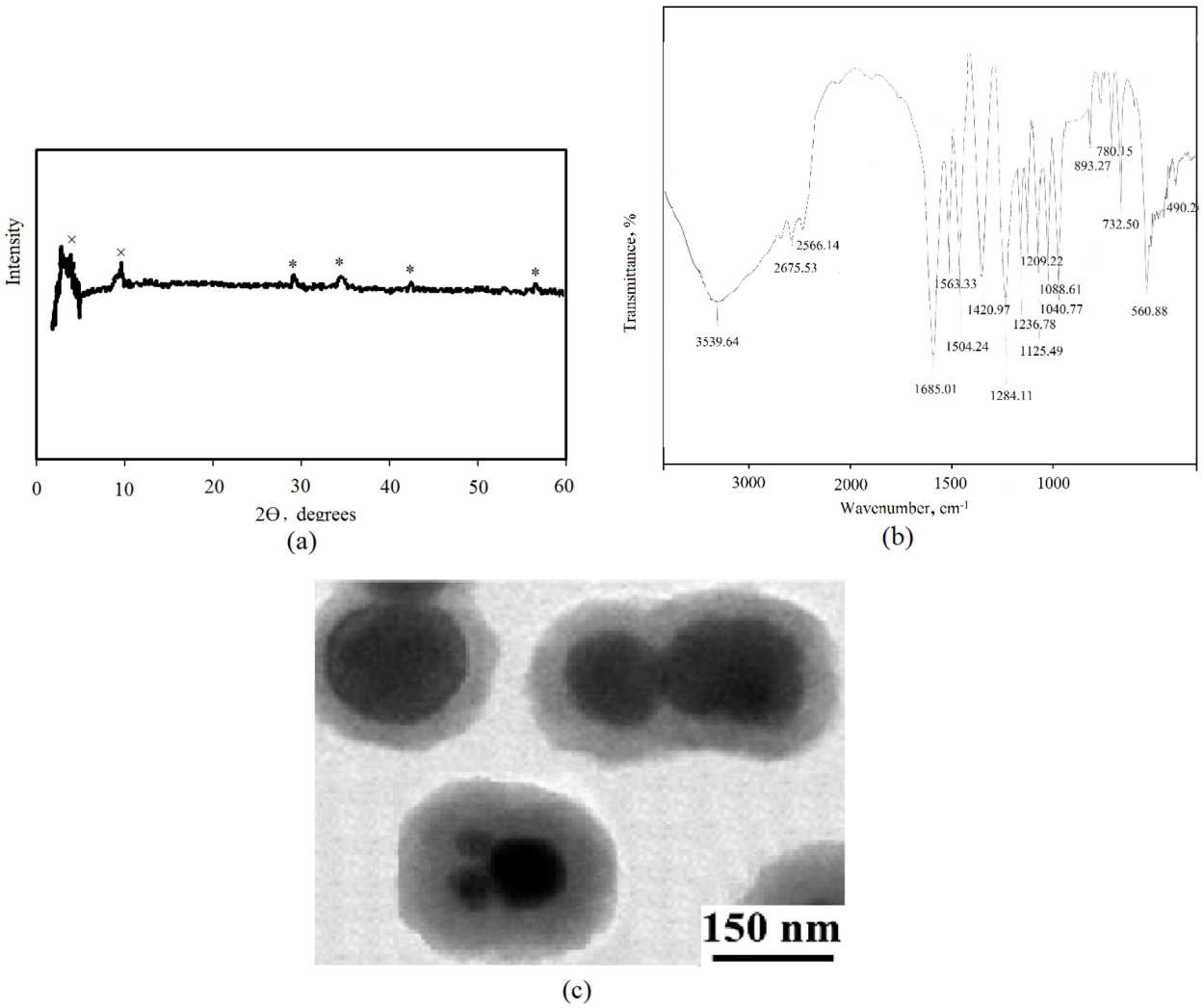

Figure 1. a) XRD pattern, b) FT-IR spectrum, and c) TEM image of Fe_3O_4@MIL-100(Fe)-OSO_3H catalyst. Peaks shown by * in (a) indicate the presence of Fe_3O_4 and those with × indicate the presence of the MIL-100(Fe) catalyst.

wt.% of Fe_3O_4 remained up to 850 K. The TGA curves of Fe_3O_4@MIL-100(Fe)-OSO_3H and MIL-100(Fe) show that two-step weight loss occurs in the temperature region of 300–850 K. The first one (about 14.0 wt.%) was observed from 320 to 380 K, which could be assigned to the loss of the residual or absorbed water. The second weight loss occurs from 600 to 800 K, which was assigned to the decomposition of the MOF. According to the mass loss in TGA of Fe_3O_4@MIL-100(Fe)-OSO_3H and MIL-100(Fe), about 14 wt.% of Fe_3O_4@MIL-100(Fe)-OSO_3H is iron oxide nanoparticles.

The optical absorption property of a semiconductor, related to its electronic structure, is recognized as one of the most important factors in determining its photocatalytic activity. The diffuse reflectance absorption spectra of the Fe_3O_4@MIL-100(Fe)-OSO_3H and iron oxide nanoparticle catalysts are shown in Figure 3a. As is clear, the absorption band of Fe_3O_4@MIL-100(Fe)-OSO_3H, in comparison to the iron oxide nanoparticles, showed an increase in absorption from 200 to 550 nm. Furthermore, based on the absorption spectrum (Figure 3a), the plot of the transformed Kubelka–Munk function of light energy $(\alpha h\upsilon)^{1/2}$ versus energy $(h\upsilon)$ for both

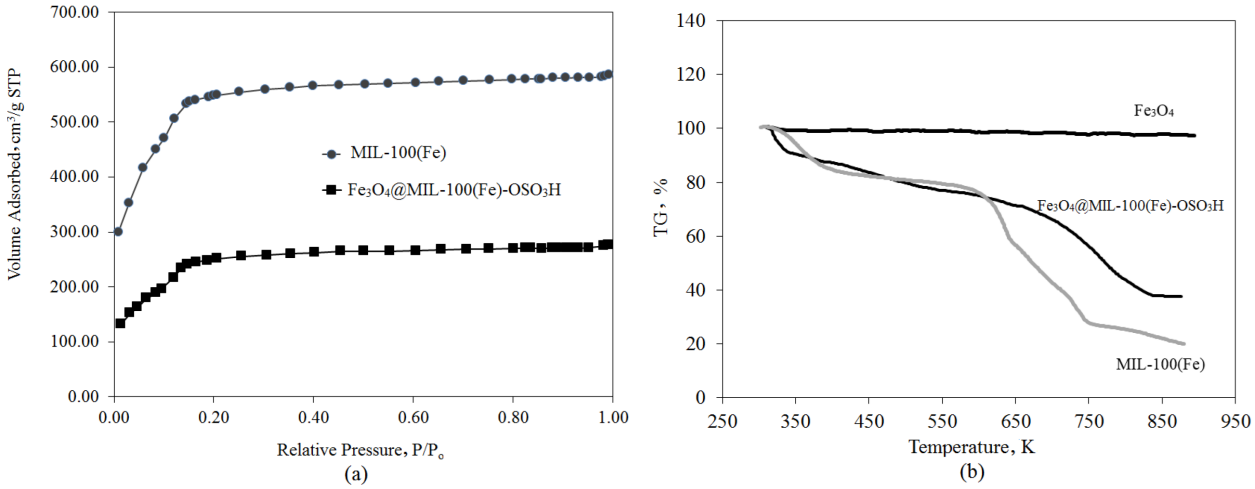

Figure 2. a) BET adsorption–desorption isotherms of MIL-100(Fe) and Fe_3O_4@MIL-100(Fe)-OSO_3H, b) DTA/TG images of Fe_3O_4, Fe_3O_4@MIL-100(Fe)-OSO_3H and MIL-100(Fe).

catalysts was constructed (Figure 3b) and the band-gap energy for Fe_3O_4@MIL-100(Fe)-OSO_3H and Fe_3O_4 NPs was found to be approximately 2.32 and 2.43 eV, respectively. The reduction in band gap energy and the enhancement of the absorption intensity for the Fe_3O_4@MIL-100(Fe)-OSO_3H catalyst, in comparison to the iron oxide nanoparticles, indicated that its photocatalytic activity has some improvement.

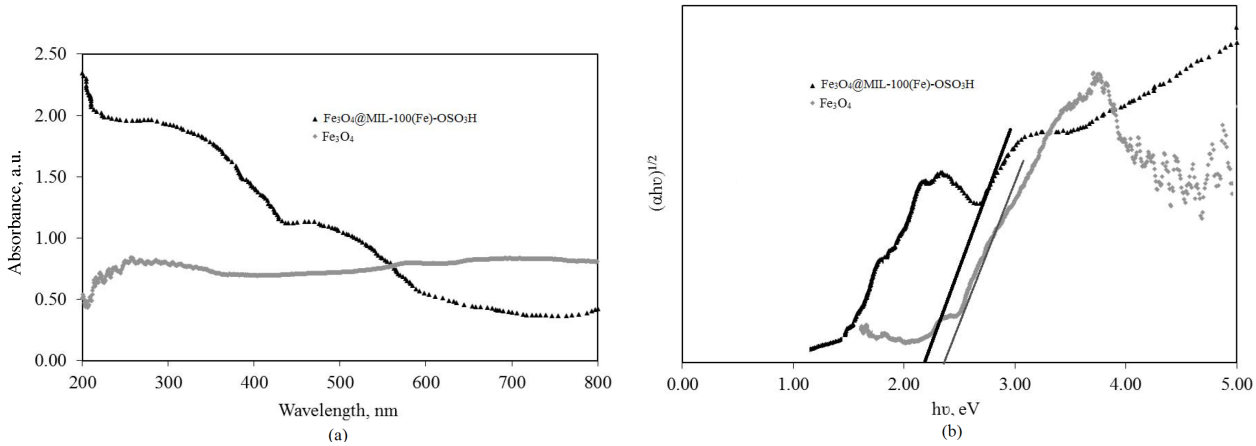

Figure 3. a) UV-vis diffuse reflectance spectra, b) plots of $(\alpha h\nu)^{1/2}$ versus photon energy($h\nu$) of Fe_3O_4 NPs and Fe_3O_4@MIL-100(Fe)-OSO_3H samples.

2.2. Effect of nature of degradation system and degradation time

In the initial experiment, the effects of MW, MW/Fe_3O_4, MW/Fe_3O_4@MIL-100(Fe), and MW/Fe_3O_4@MIL-100(Fe)-OSO_3H on degradation efficiency of MO under the experimental conditions of H_2O_2 (40 mg/L), MO initial concentration (100 mg/L), microwave power of 500 W, solution pH of 5.0, and catalyst concentration of 0.4 g/L were investigated and the results are presented in Figure 4a.

As shown in Figure 4, the concentration of MO in all the degradation systems decreased during the first 6 min of irradiation and then remained constant, so for further experiments, a period of 6 min was selected as the

optimum time of irradiation. Moreover, the results revealed that among these systems the MW/Fe_3O_4@MIL-100(Fe)-OSO_3H was more effective in the degradation of MO and 88.5% of MO was degraded in 6 min while only 2.3%, 12.5%, and 67.2% was degraded by the MW, MW/Fe_3O_4, and MW/Fe_3O_4@MIL-100(Fe) systems, respectively. The higher catalytic activity of Fe_3O_4@MIL-100(Fe)-OSO_3H can be described on the basis that Fe_3O_4 nanoparticles have high affinity for the absorption of MW irradiation[45] and production of high heat energy helps the degradation of MO. Furthermore, the oxygen atoms belonging to the sulfonate group of Fe_3O_4@MIL-100(Fe)-OSO_3H are in an electron-deficient state, which can effectively promote the separation of photoinduced electron–hole pairs and then enhance its catalytic quantum efficiency.

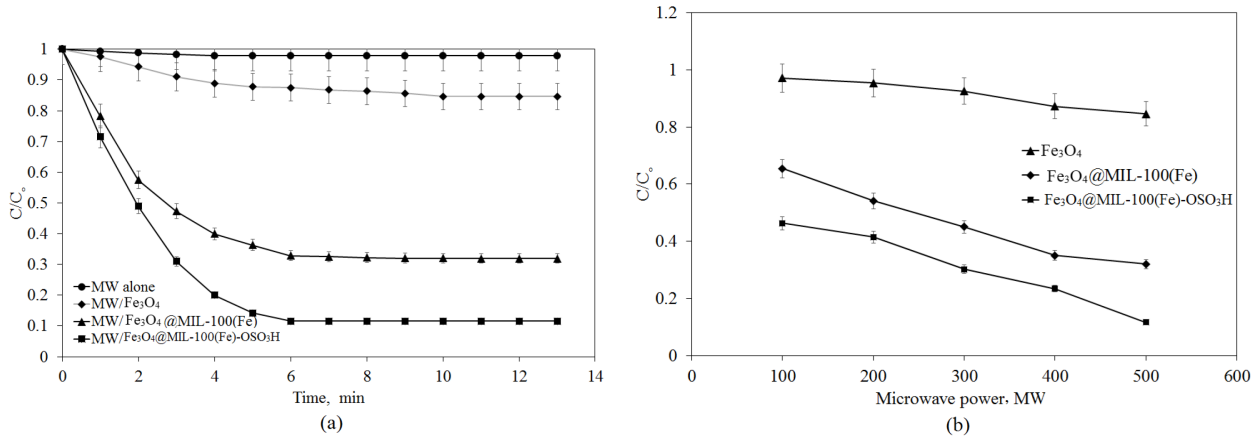

Figure 4. a) Influence of microwave irradiation (500 W) time on MO degradation efficiency, b) effect of microwave power on MO degradation (MO concentration, 100 mg/L: H_2O_2 concentration, 40 mg/L; solution pH, 5.0; catalyst concentration, 0.4 g/L).

2.3. Influence of microwave power

Microwave power, as the only energy source in the microwave-enhanced Fenton-like degradation process, can be a crucial factor in the degradation of pollutants. The effect of the microwave power on the degradation of MO by Fe_3O_4, Fe_3O_4@MIL-100(Fe), and Fe_3O_4@MIL-100(Fe)-OSO_3H was studied by varying the microwave power within the range of 100–500 W. Due to instrumental limitations, no higher power was considered. It was found that the MO degradation increased with an increase in microwave power (Figure 4b). This is because at a higher microwave power the formation of "hot spots"[42] on the surface of MOFs and $HO^{\cdot}$ radical in the aqueous solution is enhanced, which results in the higher degradation efficiency of MO. Furthermore, the extent of degradation with microwave power was always higher with the Fe_3O_4@MIL-100(Fe)-OSO_3H /MW system. Hence, in subsequent experiments, a microwave power of 500 W combined with the Fe_3O_4@MIL-100(Fe)-OSO_3H catalyst was used.

2.4. Microwave-enhanced degradation kinetics

The decomposition kinetics of MO with the microwave-enhanced Fenton-like degradation process followed an exponential decay (Figure 5a) and was analyzed by fitting the data to the pseudo first- and pseudo second-order rate equations.[46]

The plot of $\ln(C_\circ/C)$ versus time (Figure 5b) was linear with R^2 greater than 0.99, suggesting that the microwave-enhanced degradation reaction follows the pseudo first-order reaction kinetics. The reaction

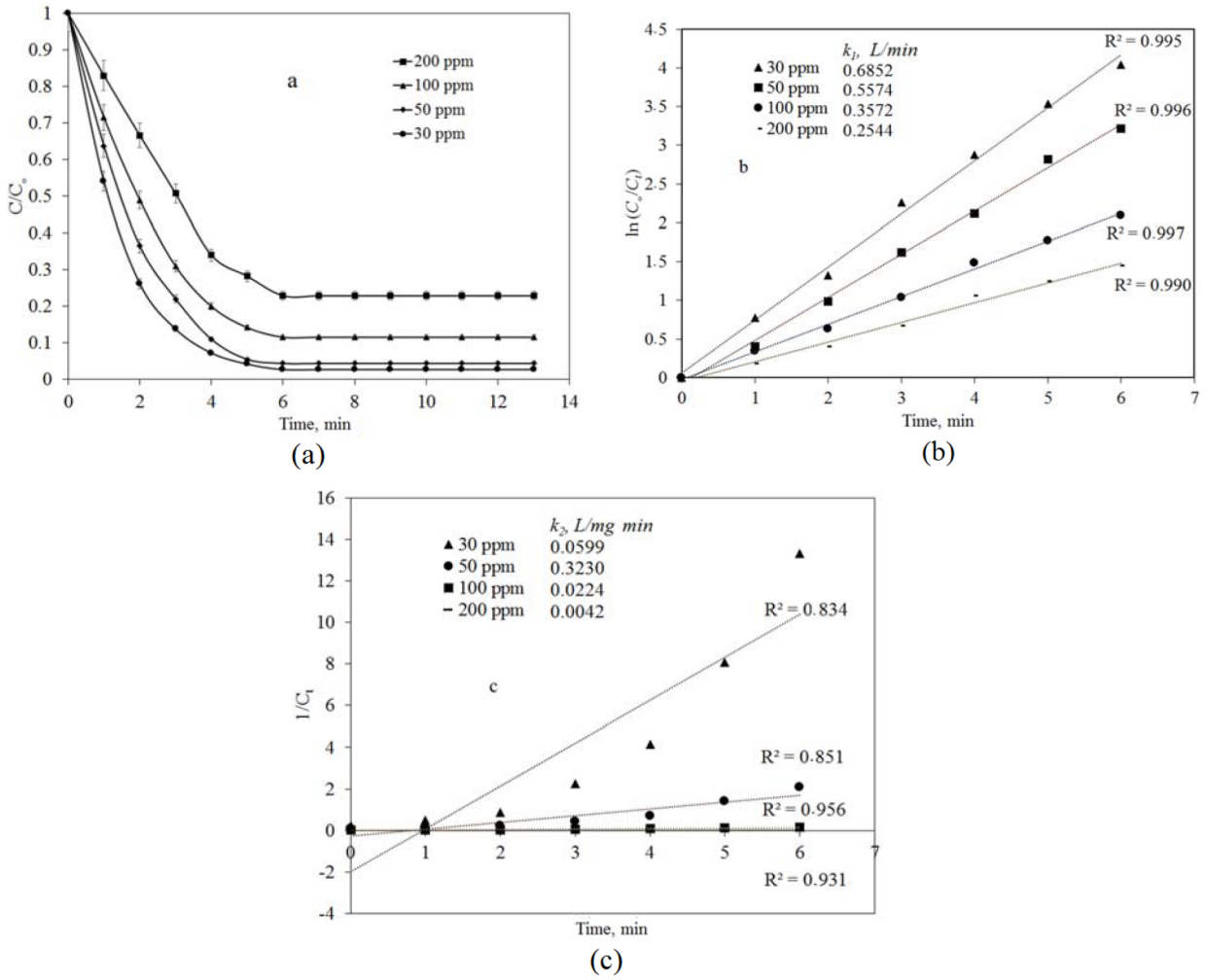

Figure 5. a) Influence of initial concentration on MO degradation efficiency, b) and c) linear plots and kinetic constants of the pseudo first-order and pseudo second-order models for MO degradation by Fe_3O_4@MIL-100(Fe)-OSO_3H (initial concentration of MO, 30–200 mg/L; initial concentration of H_2O_2, 40 mg/L; microwave power, 500 W; catalyst concentration, 0.4 g/L; pH, 5.0).

rate constants for pseudo first-order and pseudo second-order reactions were calculated and are represented in Figures 5b and 5c, respectively. The high rate constant of the pseudo first-order reaction demonstrated that the microwave-enhanced Fenton-like degradation of MO is rapid.[15,21]

2.5. Effect of MO initial concentration

From a mechanistic and application point of view, it is important to investigate the effect of substrate concentration on catalytic reaction efficiency. Experiments were conducted with varying MO concentrations in the range of 30 to 200 mg/L while keeping the other conditions constant (H_2O_2 (40 mg/L); microwave power (500 W); catalyst concentration (0.4 g/L); and pH of 5.0). The results (Figure 5a) showed that at a given time the decolorization of MO decreased with an increase in the initial concentration of MO. This could be because an increase in the initial concentration of dye causes more dye molecules to be adsorbed into the surface of the Fe_3O_4@MIL-100(Fe)-OSO_3H catalyst so that the microwave-generated holes or hydroxyl radicals are

not sufficient for direct contact with the sorbed dye molecules in the reaction. Furthermore, at higher concentrations, the dye molecules adsorb more microwave energy and so less energy reaches the catalyst surface. Thus, the combination of these effects causes a decrease in the degradation efficiency of MO at higher initial concentrations.

2.6. Effect of catalyst concentration

The use of the optimum concentration of catalyst is important for the extent of the degradation and economical removal of dye. The effect of concentration of Fe_3O_4@MIL-100(Fe)-OSO_3H in the range of 0.1–1.2 g/L was studied on the efficiency of decolorization of MO while the other experimental factors were kept constant. It was observed (Figure 6a) that an increase in the concentration of the catalyst up to 0.4 g/L causes a rapid increase in the degradation of the dye up to 88.5% and then it approximately reaches a plateau with further increase in the concentration of catalyst. This is because a larger amount of catalyst offers more active sites that accelerate the generation of $HO^{\cdot}$ and thereby it promotes the degradation efficiency of MO. Thus, an amount of 0.4 g/L of catalyst is able to produce sufficient amounts of $HO^{\cdot}$ for degradation of MO. Consequently, 0.4 g/L of Fe_3O_4@MIL-100(Fe)-OSO_3H was adopted as the optimal catalyst concentration.

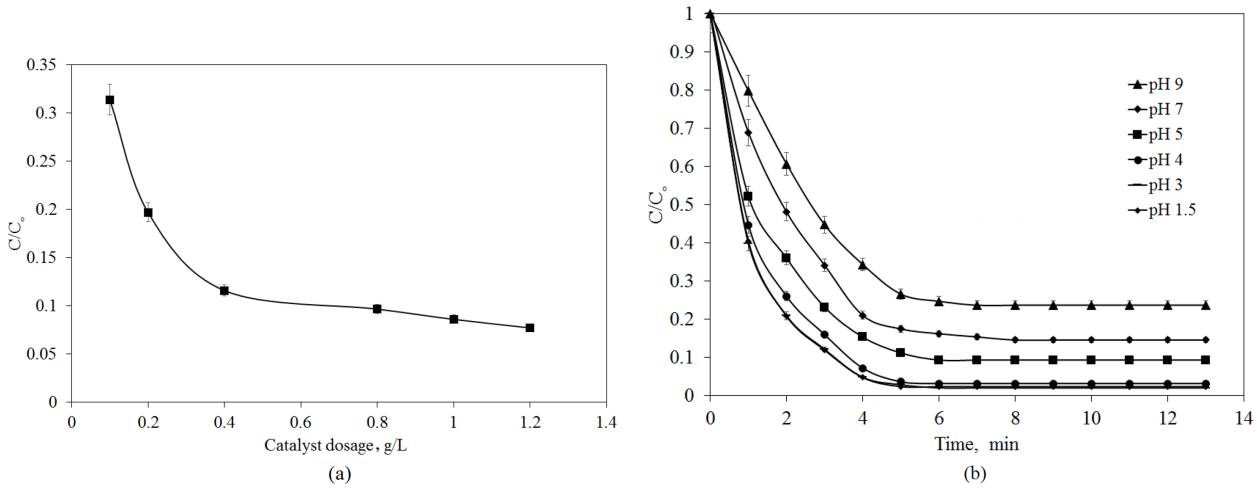

Figure 6. a) Influence of concentration of the catalyst on MO degradation efficiency at pH of 5, b) influence of solution pH on MO degradation efficiency in the presence of catalyst (0.4 g/L) (initial concentration of MO, 100 mg/L; initial concentration of H_2O_2, 40 mg/L; microwave power, 500 W; contact time, 6 min).

2.7. Effect of pH

The influence of the pH of the solution on the degradation of MO in the microwave-enhanced Fenton-like process with Fe_3O_4@MIL-100(Fe)-OSO_3H as the heterogeneous catalyst was studied by varying the pH in the range of 1.5 to 9.0 and the results are presented in Figure 6b. It was observed that the microwave-enhanced degradation of MO was significantly influenced by pH and the degradation efficiency decreased with increasing pH value. A possible explanation for this observation is that, in alkali media, H_2O_2 loses its oxidizing ability due to its decomposition to H_2O and O_2 and the charge of the MOF becomes negative, which decreases its affinity for the sorption of MO (having a negative SO_4^{2-} group). Moreover, as the efficiency of degradation of MO at pH levels of 3.0 and 1.5 was similar ($\sim$98.0 %), a pH of 3.0 was selected as the optimum pH in the subsequent work.

2.8. Effect of H_2O_2 concentration

The effect of the H_2O_2 concentration, the main source of $HO^{\cdot}$ radicals in the Fenton-like system, on the decolorization of MO was also investigated by varying its concentration within the range of 0–70 mg/L while keeping the other experimental factors at optimum levels. The results (Figure 7) showed that the MO degradation efficiency increases from 22.9% to 98.0% with increasing H_2O_2 concentration from 0 to 40 mg/L; however, further increase in H_2O_2 concentrations had no significant effect on the process. This is because an increase in H_2O_2 to a certain level can cause the increase in $HO^{\cdot}$ radicals and thereby it increases the degradation of MO.[47] Therefore, an initial concentration of 40 mg/L was chosen as the optimum H_2O_2 concentration in subsequent experiments.

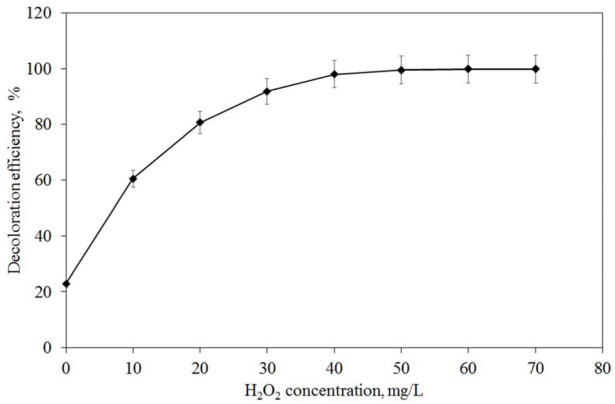

Figure 7. The effect of initial H_2O_2 concentration on MO degradation efficiency (initial concentration of MO, 100 mg/L; catalyst concentration, 0.4 g/L; microwave power, 500 W; contact time, 6 min; pH, 3.0).

2.9. Recycling of catalyst

The reusability of a catalyst adds to the favorability of the process by reducing the total cost of the process. Consequently, reusing a catalyst is very important and has great significance in its usefulness. To evaluate the reusability of the catalyst (Fe_3O_4@MIL-100(Fe)-OSO_3H), a recycling process was carried out for the degradation of MO over Fe_3O_4@MIL-100(Fe)-OSO_3H/MW in the presence of H_2O_2. After the decomposition process was completed, the Fe_3O_4@MIL-100(Fe)-OSO_3H catalysts were separated from the solution mixture by the application of an external magnetic field, washed with ethanol, and vacuum-dried at 55 °C before commencement of the next cycles. The results revealed that after ten cycles the efficiency of the degradation was more than 90.0%, indicating that the catalytic activity of Fe_3O_4@MIL-100(Fe)-OSO_3H is stable and it is reusable for at least ten cycles.

2.10. Degradation mechanism

Microwave irradiation combined with MOFs (modified with iron oxide nanoparticles and a sulfonate group) resulted in the degradation of MO, a process referred to as microwave-enhanced Fenton-like degradation. The MO degradation mechanism can be based on the presence of Fe_3O_4 nanoparticles in the MOF structure, as expressed in Eqs. (1)–(4). Thus, the MO degradation over the Fe_3O_4@MIL-100(Fe)-OSO_3H catalyst is initiated by the activation of H_2O_2 through a Fenton-like mechanism to produce the intermediate $HOO^{\cdot}$ and

$HO^{\cdot}$ radicals, which then degrade the MO (Eq. (4)).

$$Fe^{3+} + H_2O_2 \rightarrow Fe^{2+} + HOO^{\cdot} + H^{+} \quad (1)$$

$$Fe^{2+} + H_2O_2 \rightarrow Fe^{3+} + HO^{\cdot} + {}^{-}OH \quad (2)$$

$$Fe^{3+} + HOO^{\cdot} \rightarrow Fe^{2+} + O_2 + OH^{+} \quad (3)$$

$$HO^{\cdot} + \text{methyl orange} \rightarrow \text{degradation products} \quad (4)$$

The role of different parts of the Fe_3O_4@MIL-100(Fe)-OSO_3H/MW catalyst system that are involved in microwave-enhanced Fenton-like degradation can be explained as follows: 1) the Fe_3O_4 NPs in the Fe_3O_4@MIL-100(Fe)-OSO_3H structure help with degradation of the dye in the solution through the absorption of microwaves and generation of high heat. 2) The sulfonate group of the MOFs forms a new trap-state inside the band gap of Fe_3O_4@MIL-100(Fe), which promotes the electron transfer between the sulfonate group and Fe_3O_4@MIL-100(Fe) at the interface. The same results were observed for sulfonate-doped TiO_2 [48] and sulfonate-doped α-Fe_2O_3 [45] photocatalysts. 3) The MOF structure can enhance the dye degradation through a metal–oxo cluster excitation mechanism.[38] The Fe(III)-O clusters on the surface of Fe_3O_4@MIL-100(Fe)-OSO_3H can catalyze the decomposition of H_2O_2 to produce more $HO^{\cdot}$ radicals. 4) The ordered porous structure and the high surface area of Fe_3O_4@MIL-100(Fe)-OSO_3H create more catalytic sites to provide extra pathways for the migration of electrons and allow better contact between reactants and active sites, and finally the separation of charge carriers is facilitated. The MO molecules could be easily sorbed to the surface of Fe_3O_4@MIL-100(Fe)-OSO_3H by different interactions. Such adsorption increases the effective concentration of MO molecules significantly near the surfaces of the Fe_3O_4@MIL-100(Fe)-OSO_3H. 5) Moreover, as reported in the literature,[15] microwaves are able to promote the generation of hydroxyl radicals through the decomposition of H_2O_2, leading to the improvement of the oxidative capacity of the system. The general scheme for microwave-enhanced Fenton-like degradation of MO is presented in Figure 8.

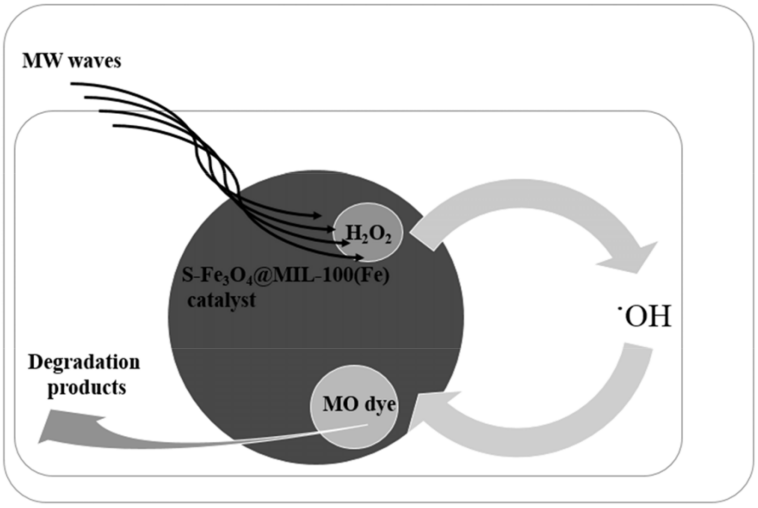

Figure 8. The diagram of microwave-enhanced Fenton-like degradation of methyl orange (MO).

Moreover, in comparison[49–52] with the other methods used in the degradation of MO, the application of microwave-enhanced Fenton-like degradation by Fe_3O_4@MOF-235(Fe)-OSO_3H has the advantages of high degradation efficiency, reusability, and fast kinetics.

2.11. Conclusions

The present work reports the fabrication of the Fe_3O_4@MIL-100(Fe)-OSO_3H composite by a facile, efficacious, and environmentally friendly method. The morphology and structure of the catalyst were studied by XRD, BET, TEM, TGA, FT-IR, and DRS analyses. The catalytic activity of the sulfonated MOF loaded on the iron oxide catalyst composite was examined by the degradation of MO in aqueous solutions under microwave irradiation. It was shown that microwave irradiation improved the efficiency of the Fenton-like degradation process by the surface-modified MOF catalyst. The kinetics of the microwave degradation follow a pseudo first-order model and MO degradation efficiency depends on several factors such as the initial MO concentration, concentration of the catalyst, microwave power, pH, and concentrations of H_2O_2 oxidants. Compared with conventional heating, it can be claimed that the kinetics and efficiency of Fenton-like degradation of dye by microwave irradiation have been improved.

3. Experimental

3.1. Materials

The reactants of $FeCl_3 \cdot 6H_2O$ (99 wt.%) as the metal source, modifying agent, trimethyl 1,3,5-benzenetricarboxylate (99 wt.%) as the organic linker, deionized water as the solvent, aminomethanesulfonic acid (AMSA, 98%), mercaptoacetic acid (MAA, 99 wt.%), magnetic iron oxide nanoparticles (Fe_3O_4 NPs, 99 wt.%), and ethanol (C_2H_5OH, 99 wt.%) were all purchased from Merck (Darmstadt, Germany) and were used for the preparation of Fe_3O_4@MIL-100(Fe)-OSO_3H.

Methyl orange (MO; C.I. 13025; molecular weight 327.33 g/mol; molecular formula $C_{14}H_{14}N_3NaO_3S$; purity 98%) was supplied by Sigma-Aldrich (98 wt.%, St. Louis, MO, USA) and was used without any further purification. A stock solution of 1000 mg/L of MO was prepared by dissolving MO in double-distilled water. Experimental solutions with desired concentrations were obtained by successive dilutions of the stock solution.

3.2. Catalyst preparation

The Fe_3O_4@MIL-100(Fe) catalyst was prepared as described in our previous study.[44] The sulfonated MOF loaded on iron oxide nanoparticles (Fe_3O_4@MIL-100(Fe)-OSO_3H) was synthesized according to the method given in the literature for sulfonation of MIL-100(Cr).[53] Thus, in a typical procedure, 0.5 g of Fe_3O_4@MIL-100(Fe) was suspended in 30 mL of absolute ethanol and 1 mmol (0.0056 g) AMSA was added. The mixture was refluxed for 12 h with continuous stirring. The product was filtered, washed with deionized water, and dried at room temperature.

3.3. Instrumentation

The porous structures of the prepared nanomaterials were studied by powder XRD (Philips 1830 diffractometer, Philips Electronic Instruments, PW 1710) using graphite-monochromated Cu Kα radiation. The BET surface area was measured with an ASAP1010M apparatus (Micrometrics Instrument Corp., USA). Thermal analysis was carried out using the STA503 (Bähr Thermoanalyse GmbH, Hüllhorst, Germany) with instrument settings

of heating rate of 10 °C/min and nitrogen atmosphere with 100 mL/min flow rate. TEM analysis was conducted with a JEM 2100 transmission electron microscope (JEOL, Japan) at 200 kV. A UV-Vis spectrophotometer (CE 2501, CECIL Instruments, Cambridge, UK) with 1.0 cm glass cuvettes was used for the measurement of absorbance at 500 and 460 nm for pH of $\leq$3.0 and $\geq$4.0, respectively. The pH of the solutions was measured with a Metrohm 780 pH meter (Metrohm Co., Herisau, Switzerland). The FT-IR spectrum of the materials in the wavenumber range of 400–4000 cm^{-1} was obtained using the KBr pellet technique with a DIGILAB FTS 7000 spectrometer (Varian, Cambridge, MA, USA) equipped with an attenuated total reflection cell. A Shimadzu spectrophotometer (2501 PC model, Kyoto, Japan) was used to record the UV-Vis diffuse reflectance spectra of the samples in the region of 200 to 800 nm. A microwave oven (WD750B, Guangdong Galanz Company, China) with a frequency of 2450 MHz and a maximum output power of 700 W was used for the irradiation.

4. Procedures

MO solution (50 mL, 100 mg/L) with pH of 5 and 20 mg of Fe_3O_4@MIL-100(Fe)-OSO_3H (0.4 g/L) were added into a Teflon-lined reactor equipped with a condenser and agitated for 300 min to reach the sorption equilibrium. Then 5.0 mL of H_2O_2 (40 mg/L) was added in order to start the Fenton-like reaction. The pH of the reaction mixture was adjusted by 0.1 M HCl solution and the system was installed in a controllable microwave oven. All experiments were conducted in batch mode. For comparison, degradation of MO in aqueous solution was also carried out by Fe_3O_4@MIL-100(Fe)-OSO_3H and MW alone. After the irradiation and separation of the catalyst by application of an external magnet, the concentration of MO was determined with a UV-Vis spectrophotometer. Maximum absorption wavelengths of MO solution at pH of $\leq$3.0 and $\geq$4.0 were 500 and 460 nm, respectively. The molar absorption coefficient (ε) of MO at 464 and 500 nm in water was measured and found to be 2.16 $\times$ 10^4 L/(mol cm) and 2.32 $\times$ 10^4 L/(mol cm), respectively. The decolorization efficiency was calculated according to the following equation:

$$\text{Decoloration efficiency}\,\% = \frac{(C_\circ - C_t)}{C_\circ} \times 100 \tag{5}$$

where $C_\circ$ and C_t are the initial and instant (at any time during reaction) concentrations of MO solution, respectively. After the reaction was completed, the catalyst was recovered by application of an external magnetic field, washed with ethanol, vacuum-dried at 55 °C, and used in the processing of the next sample.

References

1. Gupta, V. K.; Khamparia, S.; Tyagi, I.; Jaspal, D.; Malviya, A. *Glob. J. Env. Sci. Man.* **2015**, *1*, 71-94.
2. Tsuboy, M. S.; Angeli, J. P. F.; Mantovani, M. S.; Knasmüller, S.; Umbuzeiro, G. A.; Ribeiro, L. R. *Toxicol. In Vitro* **2007**, *21*, 1650-1655.
3. Hassanzadeh-Tabrizi, S. A.; Mohaghegh Motlagh, M.; Salahshour, S. *App. Surf. Sci.* **2016**, *384*, 237-243.
4. Karadai, A. *Turk. J. Chem.* **1998**, *22*, 227-236.
5. Parsa, J. B.; Chianeh, F. N. *Korean J. Chem. Eng.* **2012**, *29*, 1585-1590.
6. Al-Bastaki, N. *Chem. Eng. Process.* **2004**, *43*, 1561-1567.
7. Maleki, A.; Mahvi, A. H.; Ebrahimi, R.; Zandsalimi, Y. *Korean J. Chem. Eng.* **2010**, *27*, 1805-1810.
8. Akarsu, M.; Asiltürk, M.; Sayılkan, F.; Kiraz, N.; Arpaç, E.; Sayılkan, H. *Turk. J. Chem.* **2006**, *30*, 333-342.

9. Khataee, A.; Fathinia, M.; Bozorg, S. *Turk. J. Chem.* **2016**, *40*, 347-363.
10. Liu, Z.; Wang, F.; Li, Y.; Xu, T.; Zhu, S. *J. Environ. Sci.* **2011**, *23*, S70-S73.
11. Liu, C.; Xu, H.; Li, H.; Liu, L.; Xu, L.; Ye, Z. *Korean J. Chem. Eng.* **2011**, *28*, 1126-1132.
12. Liu, Y.; Sun, D. *Appl. Catal. B* **2007**, *72*, 205-211.
13. Andreozzi, R.; Caprio, V.; Insola, A.; Marotta, R. *Catal. Today* **1999**, *53*, 51-59.
14. Garrido-Ramírez, E. G.; Theng, B. K. G.; Mora, M. L. *Appl. Clay Sci.* **2010**, *47*, 182-192.
15. Pan, W.; Zhang, G.; Zheng, T.; Wang, P. *RSC Adv.* **2015**, *5*, 27043-27051.
16. Arslan-Alaton, I.; Tureli, G.; Olmez-Hanci, T. *J. Photochem. Photobiol. A* **2009**, *202*, 142-153.
17. Zhang, H.; Fu, H.; Zhang, D. *J. Hazard. Mater.* **2009**, *172*, 654-660.
18. Zhao, G.; Peng, X.; Li, H.; Wang, J.; Zhou, L.; Zhao, T.; Huang, Z.; Jiang, H. *Chem. Commun.* **2015**, *51*, 7489-7492.
19. Yang, S.; Yang, L.; Liu, X.; Xie, J.; Zhang, X.; Yu, B.; Wu, R.; Li, H.; Chen, L.; Liu, J. *Sci. China Technol. Sc.* **2015**, *58*, 858-863.
20. Basso, A.; Sinigoi, L.; Gardossi, L.; Flitsch, S. *Int. J. Pept.* **2009**, *2009*, 1-4.
21. Yin, C.; Cai, J.; Gao, L.; Yin, J.; Zhou, J. *J. Hazard. Mater.* **2016**, *305*, 15-20.
22. Nidheesh, P. V.; Gandhimathi, R.; Velmathi, S.; Sanjini, N. S. *RSC Adv.* **2014**, *4*, 5698-5708.
23. Ricco, R.; Konstas, K.; Styles, M. J.; Richardson, J. J.; Babarao, R.; Suzuki, K.; Scopece, P.; Falcaro, P. *J. Mater. Chem. A*. **2015**, *3*, 19822-19831.
24. Shen, J.; Yang, H.; Shen, Q.; Feng, Y.; Cai, Q. *CrystEngComm* **2014**, *16*, 1868-1872.
25. Li, L.; Zhao, J.; Yang, J.; Fu, T.; Xue, N.; Peng, L.; Guo, X.; Ding, W. *RSC Adv.* **2015**, *5*, 4766-4769.
26. Chamnankid, B.; Föttinger, K.; Rupprechter, G.; Kongkachuichay, P. *Chem. Eng. Technol.* **2014**, *37*, 2129-2134.
27. Duarte, F.; Madeira, L. M. *Sep. Sci. Technol.* **2010**, *45*, 1512-1520.
28. Rioux, R. M.; Song, H.; Hoefelmeyer, J. D.; Yang, P.; Somorjai, G. A. *J. Phys. Chem. B* **2005**, *109*, 2192-2202.
29. Stock, N.; Biswas, S. *Chem. Rev.* **2012**, *112*, 933-969.
30. Ma, L.; Abney, C.; Lin, W. *Chem. Soc. Rev.* **2009**, *38*, 1248-1256.
31. Li, J. R.; Ma, Y.; McCarthy, M. C.; Sculley, J.; Yu, J.; Jeong, H. K.; Balbuena, P. B.; Zhou, H. C. *Coord. Chem. Rev.* **2011**, *255*, 1791-1823.
32. Ma, S.; Zhou, H. C. *Chem. Commun.* **2010**, *46*, 44-53.
33. Rodrigues, M. O.; de Paula, M. V.; Wanderley, K. A.; Vasconcelos, I. B.; Alves, S.; Soares, T. A. *Int. J. Quantum Chem.* **2012**, *112*, 3346-3355.
34. Silva, C. G.; Corma, A.; Garcia, H. *J. Mater. Chem.* **2010**, *20*, 3141-3156.
35. Llabrés i Xamena, F. X.; Corma, A.; Garcia, H. *J. Phys. Chem. C* **2007**, *111*, 80-85.
36. Wang, C. C.; Li, J. R.; Lv, X. L.; Zhang, Y. Q.; Guo, G. *Energy Environ. Sci.* **2014**, *7*, 2831-2867.
37. Lv, H.; Zhao, H.; Cao, T.; Qian, L.; Wang, Y.; Zhao, G. *J. Mol. Catal. A-Chem.* **2015**, *400*, 81-89.
38. Laurier, K. G. M.; Vermoortele, F.; Ameloot, R.; De Vos, D. E.; Hofkens, J.; Roeffaers, M. B. J. *J. Am. Chem. Soc.* **2013**, *135*, 14488-14491.
39. Liang, R.; Shen, L.; Jing, F.; Wu, W.; Qin, N.; Lin, R.; Wu, L. *Appl. Catal. B* **2015**, *162*, 245-251.
40. Gulcan, M.; Zahmakiran, M.; Özkar, S. *Appl. Catal. B* **2014**, *147*, 394-401.
41. Wu, Y.; Luo, H.; Wang, H. *RSC Adv.* **2014**, *4*, 40435-40438.
42. Yang, Y.; Wang, P.; Shi, S.; Liu, Y. *J. Hazard. Mater.* **2009**, *168*, 238-245.
43. Dalai, A. K.; Sethuraman, R.; Katikaneni, S. P. R.; Idem, R. O. *Ind. Eng. Chem. Res.* **1998**, *37*, 3869-3878.
44. Dadfarnia, S.; Haji Shabani, A. M.; Moradi, S. E.; Emami, S. *Appl. Surf. Sci.* **2015**, *330*, 85-93.

45. Guo, L.; Chen, F.; Fan, X.; Cai, W.; Zhang, J. *Appl. Catal. B* **2010**, *96*, 162-168.

46. Shahwan, T.; Abu Sirriah, S.; Nairat, M.; Boyacı, E.; Eroğlu, A. E.; Scott, T. B.; Hallam, K. R. *Chem. Eng. J.* **2011**, *172*, 258-266.

47. Ramirez, J. H.; Maldonado-Hódar, F. J.; Pérez-Cadenas, A. F.; Moreno-Castilla, C.; Costa, C. A.; Madeira, L. M. *Appl. Catal., B* **2007**, *75*, 312-323.

48. Wu, X. W.; Wu, D. J.; Liu, X. J. *Appl. Phys. A* **2009**, *97*, 243-248.

49. Chen, T.; Zheng, Y.; Lin, J.; Chen, G. *J. Am. Soc. Mass Spectrom.* **2008**, *19*, 997-1003.

50. Yu, L.; Xi, J.; Li, M.; Chan, H.T.; Su, T.; Phillips, D. L.; Chan, W. K. *Phys. Chem. Chem. Phys.* **2012**, *14*, 3589-3595.

51. Gao, X.; Jiao, X.; Zhang, L.; Zhu, W.; Xu, X.; Ma, H.; Chen, T. *RSC Adv.* **2015**, *5*, 76963-76972.

52. Lu, L.; Yang, F.; Yang, X. *Analyst* **2014**, *139*, 6122-6125.

53. Ahmed, I.; Hasan, Z.; Khan, N. A.; Jhung, S. H. *Appl. Catal. B* **2013**, *129*, 123-129.